

Thermal cum DC Camouflage in Duet with Undecorated Natural Materials

Tian-Zhi Yang^{1,2#}, Xue Bai^{1,3,4#}, Dongliang Gao¹, Linzhi Wu⁵, Baowen Li^{3,4,6}, John T. L. Thong^{1,3}, and Cheng-Wei Qiu^{1,3*}

¹Department of Electrical and Computer Engineering, National University of Singapore, Kent Ridge 119620, Republic of Singapore

²Department of Astronautics, Shenyang Aerospace University, Shenyang 110136, China

³NUS Graduate School for Integrated Sciences and Engineering, National University of Singapore, Kent Ridge 117542, Republic of Singapore

⁴Department of Physics and Centre for Computational Science and Engineering, National University of Singapore, Singapore 117546, Republic of Singapore

⁵Center for Composite Materials, Harbin Institute of Technology, Harbin 150001, China

⁶Center for Phononics and Thermal Energy Science, School of Physics Science and Engineering, Tongji University, Shanghai 200092, China

*Corresponding author: chengwei.qiu@nus.edu.sg, # Equal contribution

Abstract:

To manipulate various types of physical signals in one single device has long captivated the attention of scientists and engineers. This however is very challenging, if not impossible, even for emerging metamaterials. Up to date, many artificial materials have been proposed, theoretically and (or) experimentally, for manipulating various waves/signals on a one-function-one-device basis. In this work, for the very first time, we employ undecorated natural materials to experimentally demonstrate a simultaneous camouflage for thermal current and electric dc current on the same device. It demonstrates how ingenuity can overcome the limitations of natural material systems without the need for complex decoration to impart inhomogeneous and (or) anisotropic

properties, which was previously considered impossible to accomplish except by using metamaterials.

PACS number: 81.05.Xj, 05.70.-a, 44.90.+c, 44.10.+i

Text:

Metamaterials are man-made composites that control waves in unprecedented ways, resulting in exotic behavior absent in nature. Electromagnetic metamaterials, based on transformation optics, were proposed to manipulate electromagnetic waves and produce a cloak of invisibility [1,2]. The concept was experimentally validated at microwave frequencies [3]. This pioneering idea motivated a number of significant applications, such as concentrator [4], rotator [5], wave shifter/splitter [6] and illusion devices [7]. Besides manipulating electromagnetic wave, due to the form invariant, the transformation-based method has been extended to manipulate other waves such as acoustic and elastic waves [8-10], magnetostatic fields [11-13] and static forces [14]. More recently, metamaterials were presented to control dc current [15-17] and heat flux [18-24]. Such wave manipulations were respectively engineered on devices with different structures, materials and geometries. However, these devices were designed to control only one physical field, because it is very challenging to manipulate various types of waves with a single device.

In the development of metamaterials, the functionality has always been accompanied by complexity. In some scenarios, the more advanced devices inevitably need more complex decoration and fabrication methods. On the other hand, undecorated natural materials were dismissed as lacking versatility. For example, to realize overall inhomogeneous or/and anisotropic characteristics, electromagnetic metamaterials have been fabricated as multilayered cylinders which discretize the transformation-based cloak into many-layered coatings, and each layer is anisotropic. DC cloaking devices have been realized by using spatially varying electric resistor networks to approximately mimic the anisotropic and inhomogeneous property. Therefore, complex decoration becomes another inherent challenge to manipulate multi-waves simultaneously on one device.

More recently, some attempts to manipulate multiple physical fields in one single device have been proposed. Two theoretical works have been presented for designing an integrated device to achieve multiple functionalities [25-27]. Nevertheless, within these frameworks, the devices need a mixture of thermal and electric conductivities in each ultra-microstructure. Therefore, they require more complex synthesis, which severely restricts their realization. Shortly following these reports, an experiment was first proposed to simultaneously guide electrical current and heat flux around an air cavity [27]. This sample was fabricated by a complex artificial structure made by drilling holes into a silicon plate and filling them with polydimethylsiloxane (PDMS). Here we overcome these limitations by demonstrating an undecorated integrated device that can manipulate electric and thermal fields simultaneously. We fully utilize naturally available materials to fabricate the device that act as a "mask" in both thermal and electric fields, behaving as a multifunctional camouflage device.

Moreover, it is more interesting to add an additional function to our multifunctional camouflage device, that is, not only to behave as a camouflaging shell, but also to allow probing the external environment at the same time. In contrast, conventional cloaks prevent any thermal flux and electric current from propagating/entering into the cloaked region, thereby rendering the object completely insulated. Therefore, such a strategy might not be suitable for cloaking a sensor, which needs measure outside signals at the same time. So far, no theoretical and experimental works have been proposed on this dual physical field invisible sensing concept. Here, we experimentally realize this scientific conception on both thermal and electric fields on our device. More interestingly, our device overall can be regarded as an invisible sensor for both thermal and dc fields.

A schematic of our dual camouflage concept is shown in Figure 1. We aim to camouflage a sensor with radius a using a thin isotropic shell (with thickness $b-a$). The sensor is embedded in a background plate subjected to uniform thermal and electric fields at both ends. Such a built-in sensor could be found, for example, in a semiconductor wafer processing hotplate. Due to the discontinuity of material conductivities, the presence of the bare sensor disturbs the surrounding thermal and electric signatures. In

order to realize an invisible sensing device in both electric and thermal fields, we place a camouflaging shell that is expected to drastically reduce the perturbation of heat flux and electric current simultaneously.

To accomplish dual-field camouflage, we start by considering the electric and thermal conduction equations

$$\nabla \cdot (\kappa \nabla T) = 0, \quad \nabla \cdot (\sigma \nabla V) = 0 \quad (1)$$

where κ and T denote the thermal conductivity and temperature, and σ and V denote the electrical conductivity and electrical potential. To cloak a sensor without affecting its capability to receive an incoming signal, the concepts of "scattering cancellation" or "neutral inclusion" can be utilized, see [28-32]. the material parameters of the concealed sensor (core), shell and background in **thermal** field must satisfy (see the Supplementary Materials S1)

$$b_{thermal} = a \sqrt{\frac{(\kappa_2 - \kappa_1)(\kappa_2 + \kappa_b)}{(\kappa_2 + \kappa_1)(\kappa_2 - \kappa_b)}}, \quad (2)$$

in which a is the radius of the sensor, $b_{thermal}$ is the required radius of shell in thermal field. κ_1 , κ_2 and κ_b are thermal conductivities of sensor, shell, and background, respectively. On the other hand, the material parameters of camouflaged sensor (core), shell and background in **electric** field must satisfy

$$b_{elec} = a \sqrt{\frac{(\sigma_2 - \sigma_1)(\sigma_2 + \sigma_b)}{(\sigma_2 + \sigma_1)(\sigma_2 - \sigma_b)}}. \quad (3)$$

in which b_{elec} is the required radius of shell in electric field. σ_1 , σ_2 and σ_b are electrical conductivities of sensor, shell, and background, respectively.

Generally, thermal and dc metamaterials respectively satisfy the relationships (2) and (3), implying that the required radii of outer shells are not equal, that is, ($b_{thermal} \neq b_{elec}$).

As a result, most artificial devices are only valid for manipulating one field and serve a single-function application. In this work, we show that some natural materials can be tuned to fulfill Eqs. (2) and (3) simultaneously, which was considered not possible before [26-27]. This is due to the belief that naturally occurring materials have insufficient

flexibility. To match the geometry and material specifications in Eqs. (2) and (3) in both thermal and dc fields, we fix the radius of the sensor a and tune the outer radius b using different naturally available materials (with different thermal and electrical conductivities) to achieve $b_{thermal} = b_{elec}$. This provides a realistic route to designing a shell that can be wrapped on solid sensors to camouflage in both thermal and electric imaging.

As an example, we consider a sensor made of stainless steel is used to probe electric and thermal signal in an alloy plate (magnesium). We plot the required radii b in Figure 2(a) in both thermal and electric fields, respectively. The corresponding materials parameters are: stainless steel (with $\kappa_1=30$ W/mK, $\sigma_1=1.43\times 10^6$ S m⁻¹), copper (with $\kappa_2=400$ W/mK, $\sigma_2=5.9\times 10^7$ S m⁻¹) and magnesium alloy (with $\kappa_b=72.7$ W/mK, $\sigma_b=6.99\times 10^6$ S m⁻¹). The solid black and blue dotted lines correspond to the calculated radius for copper shell in dc and thermal fields, respectively. The orange markers and the red dotted line denote the calculated outer radius for zinc (with $\kappa_b=116$ W/mK, $\sigma_{1b}=1.7\times 10^7$ S m⁻¹) shell for thermal and dc fields, respectively. It is seen that, for a fixed sensor radius a , the radius of pure copper shell satisfies Eq. (2) and (3) simultaneously, implying that the copper shell has a dual camouflaging capability. In contrast, the Zinc shell requires different radii for thermal and electric fields, respectively, indicating that Zinc is not suitable for constructing such a shell. It should be stressed that, this tuning method can cover a wide range of different natural media. Without loss of generality, we give another example in Figure 2(b), in which we consider the sensor (probe), shell, and, background are made of lead, silver and zinc, respectively. The corresponding materials parameters are lead (with $\kappa_1=35$ W/mK, $\sigma_1=4.8\times 10^6$ S m⁻¹), silver (with $\kappa_2=410$ W/mK, $\sigma_2=6.2\times 10^7$ S m⁻¹) and zinc. The solid and the dotted lines represent the calculated radius of the shell. It shows that as the radius of sensor increases, the two lines agree well, implying that this method also allows us to camouflage a relatively larger sensor. We note that our proof-of-concept design is limited to undecorated natural materials, providing less options for material selection. In contrast, conventional metamaterials may have more degrees of freedom in creating more sophisticated devices.

We performed numerical simulations to validate the dual camouflage performance. The COMSOL Multiphysics software based on the finite element method (FEM) is used to conduct the simulation in both dc and thermal modules. We first explored the performance of our design in thermal field. The simulation result of thermal camouflage is shown in Figure 3(a1), in which the vertical lines represent the isothermal contour. When the sensor (with radius $a=15\text{mm}$) is wrapped with the shell (with radius $b=16.52\text{mm}$), there is no obvious thermal signature appearing in the infrared image, as if no sensor were there. The camouflaged sensor smoothly merges with the background. The isothermal lines are straight and parallel in the core, shell and background regions, indicating that the heat flux can penetrate the shell and the temperature gradient is uniform everywhere. This feature is drastically different from the conventional thermal cloaking, in which the cloaking region inside the shell is isolated from the external surroundings. However, as a result of blocking heat flux, the heat signature looks "cold" in the thermal image, making the sensor detectable out of plane, though undetectable in-plane. Our design renders the sensor completely invisible with the camouflage concept, and at the same time allows the sensor to observe the external environment.

In Figure 3(a2), a bare sensor, as a reference sample, was simulated. The bare sensor, as a poor conductor, strongly attracts and bends the isothermal lines toward it. As a result, the presence of the sensor distorts the surrounding thermal fields, exhibiting an obvious heat signature in thermal imaging. The sensor can be easily captured and observed by an outside observer, using equipment such as infrared cameras. Moreover, the sensor receives an inaccurate temperature signal in the distorted field.

For experimental verification, we fabricated samples through an electrical discharge machining (EDM) process, through which grooves were cut on a magnesium alloy plate of 3mm thickness. The core was assembled tightly to exclude air at the interface. The temperature measurement was taken at 10 minutes for achieving steady-state. We measured the temperature profile macroscopically using an infrared camera (FLIR i60). Both the camouflaged and the bare sensors were measured. A constant temperature gradient was imposed across the samples through a hot side being maintained using a heater at 333 K and the cold side being an ice-water mixture, held at 273 K. The top and

bottom edges were insulated. Figure 3(b1) shows the fully camouflaged sensor in thermal field. As expected, the coated sensor smoothly fits the surrounding thermal fields. As the result, the thermal signature of the sensor disappears entirely. Without marking the position of the sensor, one almost cannot observe and localize it. This camouflage result is remarkably different from previous dc [15-17] and thermal cloak [18-24], which routes the heat flux around the object and looks the object much cooler in the thermal signature. In contrast, here we make the sensor truly invisible in the thermal signature. In contrast, strongly perturbed heat diffusion was observed for the bare sensor in Figure 3(b2). The isothermal lines are obviously bent as heat flux propagates through the bare sensor. The bare sensor automatically appears in the observed thermal signature, thus it is easy to see the shape, size and position of the sensor. Remarkably, the agreements between the simulation and experimental results in Figure 3 are good. The snapshots of time-dependent camouflage performance can be seen in a movie (Supplementary Material S2).

We next measured the camouflage performance in electric field for the same sample. The potential distribution of electric field was taken at room temperature 20 °C. As the overall sample is a good electric conductor, we used a powerful dc current source and flowed a large electric current (8A) through the sample to obtain noise-free voltage measurements. The voltage at each node was manually measured and the final data was processed in the MATLAB environment. To obtain stable and accurate data, the measured values V_i were tested five times at each node, and then normalized to the total potential V_{total} value between the two boundaries. Figure 4 (a1,a2) depict the simulated potential distribution for the coated and bare sensors. A constant voltage was imposed on the left and right boundaries of the whole sample. The top and bottom boundaries were physically insulated. Figure 4(a1) shows the potential contour on the sample, in which the solid lines refer to the equipotential lines. It is seen that they are straight and parallel everywhere. The electric current can smoothly enter and pass through the sensor without disturbing the original trajectories, rendering the sensor entirely invisible. As a result, the sensor is concealed in the background and cannot be detected or localized. In contrast, as shown in Figure 4(a2), the bare sensor causes a strong disturbance of the electric field. In the

vicinity of the sensor, the equipotential lines are strongly bent. Therefore, the sensor can be easily detected using electrical impedance scanning, via the recorded contrast.

In order to quantitatively measure the camouflage performance in electric field, as shown in Figure 4(b1,b2), we probed the potential distribution using a Keithley 2000 multimeter. As shown in Figure 4(b1), the shell eliminates the “shadow” in the near-field and the sensor smoothly fits the outside electric fields, exhibiting a good camouflage performance. The electric current "scattering" is greatly suppressed around the sensor. The presence of the coated sensor does not disturb the surrounding electric field. Therefore, the sensor can measure proper voltage data. In comparison, the bare sensor (as shown in Figure 4 (b2)) strongly distorts the potential distribution. As the electric current gets closer to the sensor, the potential profile becomes more distorted. As a result, the sensor can be easily detected and localized. As expected, all these measurements are in good agreement with our theoretical predictions in Figure 4 (a1,a2).

To quantitatively confirm the camouflage performance in dc field, we also measured a close-up view of the potential distribution. We chose the '*nearest*' observation lines at $x=-1.8$ cm and right $x=1.8$ cm, as shown in Figure 5(a). It is seen that the simulated and experimental results are in good agreement. The measured potential values locate on two predicted straight lines, confirming that the sensor is in a distortion-free environment. Therefore, the above measurement further confirms that the sensor is successfully camouflaged and becomes undetectable. The camouflage shell does not reduce their capability of probing the near field. In figure 5(b), the measured potential values along the horizontal line $y=0$ increase linearly, indicating that the invisible sensor can probe the environmental potential correctly.

We have theoretically and experimentally presented a 2-dimensional isotropic shell made of naturally available materials operating in both electrical and thermal fields, providing a dual-field camouflaging capability. On the basis of these results, we explored the possibility of avoiding detection by infrared thermal imaging camera and electrical impedance scanning. The camouflage shell is very thin and homogenous, which is easy to fabricate in practice. Our device offers a practical and truly alternative avenue to explore this dual camouflaging capability. This is the first time that such dual camouflage device

has been experimentally demonstrated by using naturally undecorated materials.

C. W. Q. acknowledges Grant No. R-263-000-A23-232 administered by the National University of Singapore. T. Z. Y. acknowledges support from the National Science Foundation of China under Grant No. 11202140, 11072068 and the Program of Excellent Team at Harbin Institute of Technology.

Reference

- [1]. J.B. Pendry, D. Schurig, and D.R. Smith, *Science* **312**, 1780 (2006).
- [2]. U. Leonhardt, *Science* **312**, 1777 (2006).
- [3]. D. Schurig, et al. *Science* **314**, 977-980 (2006).
- [4]. M. Rahm, et al. *Nanostruct.* **6**, 87 (2008).
- [5]. H. Y. Chen, and C. T. Chan, *Appl. Phys. Lett.* **90**, 241105 (2007).
- [6]. M. Rahm, et al. *Phys. Rev. Lett.* **100**, 063903 (2008).
- [7]. Y. Lai, et al. *Phys. Rev. Lett.* **102**, 253902 (2009).
- [8]. L. Zigoneanu, B. Popa, and S.A. Cummer, *Nat. Phys.* **13**, 352 (2014).
- [9]. B. Popa, L. Zigoneanu, and S.A. Cummer, *Phys. Rev. Lett.* **106**, 253901 (2011).
- [10]. M. Brun, S. Guenneau, and A. B. Movchan, *Appl. Phys. Lett.* **94**, 061903 (2009).
- [11]. F. Gomory, M. Solovyov, J., Souc, C. Navau, J. Prat-Camps, and A. Sanchez, *Science* **335**, 1466 (2012).
- [12]. S. Narayana and Y. Sato, *Adv. Mater.* **24**, 71 (2012).
- [13]. B. Wood, and J.B. Pendry, *J. Phys. Condens. Matter.* **19**, 076208. (2007).
- [14]. T. Bückmann, M., Thiel, M. Kadic, R. Schittny, and M. Wegener, *Nat. Commun.* **5**, 4130 (2014).
- [15]. F. Yang, Z.L. Mei, T.Y. Jin, and T.J. Cui, *Phys. Rev. Lett.* **109**, 053902 (2012).
- [16]. W. X. Jiang, C. Y. Luo, Z.L. Mei, and T.J. Cui, *Appl. Phys. Lett.* **102**, 014102 (2013).
- [17]. T. Han, H. Ye, Y. Luo, S.P. Yeo, J.H. Teng, S. Zhang, and C.W. Qiu, *Adv. Mater.* **26**, 3478 (2014).
- [18]. C.Z. Fan, Y. Gao, and J.P. Huang, *Appl. Phys. Lett.* **92**, 251907 (2008).

- [19]. S. Guenneau, C. Amra, and D. Veynante, *Opt. Express*. **20**, 8207 (2012).
- [20]. T. Han, X. Bai, D. Gao, J.T.L.Thong , B.W. Li, and Qiu, C.W. *Phys. Rev. Lett.* **112**, 054302 (2014).
- [21]. H. Xu, X. Shi, F. Gao, H. Sun, and B.L. Zhang, *Phys. Rev. Lett.* **112**, 054301 (2014).
- [22]. S. Narayana and Y. Sato, *Phys. Rev. Lett.* **108**, 214303 (2012).
- [23]. R. Schittny, M. Kadic, S. Guenneau, and M. Wegener, *Phys. Rev. Lett.* **110**, 195901 (2013).
- [24]. U. Leonhardt, *Nature* **498**, 440 (2013).
- [25]. J. Y. Li, Y. Gao, and J. P. Huang, *J. Appl. Phys.* **108**, 074504 (2010).
- [26]. M. Moccia, G. Castaldi, S. Savo, Y. Sato, and V. Galdi, *Phys. Rev. X*. **4**, 021025 (2014).
- [27]. Y.G. Ma, Y. Liu, M. Raza, X. Wang, and S. He, *Phys. Rev. Lett.* **113**, 205501 (2014).
- [28]. A. Alù, and N. Engheta, *Phys. Rev. Lett.* **102**, 233901 (2009).
- [29]. M. D. Guild, A. Alù, and M.R. Haberman, *Appl. Phys. Lett.* **105**, 023510 (2014).
- [30]. R. Fleury, L. Sounas, and A. Alù, *Nat. Commun.* **6**, 5905, (2015).
- [31]. A. Alù, and N. Engheta, *Phys. Rev. E*. **72** 016623 (2005).
- [32]. G.W. Milton, *The theory of composites* (Cambridge University Press, 2002)

Figures 1

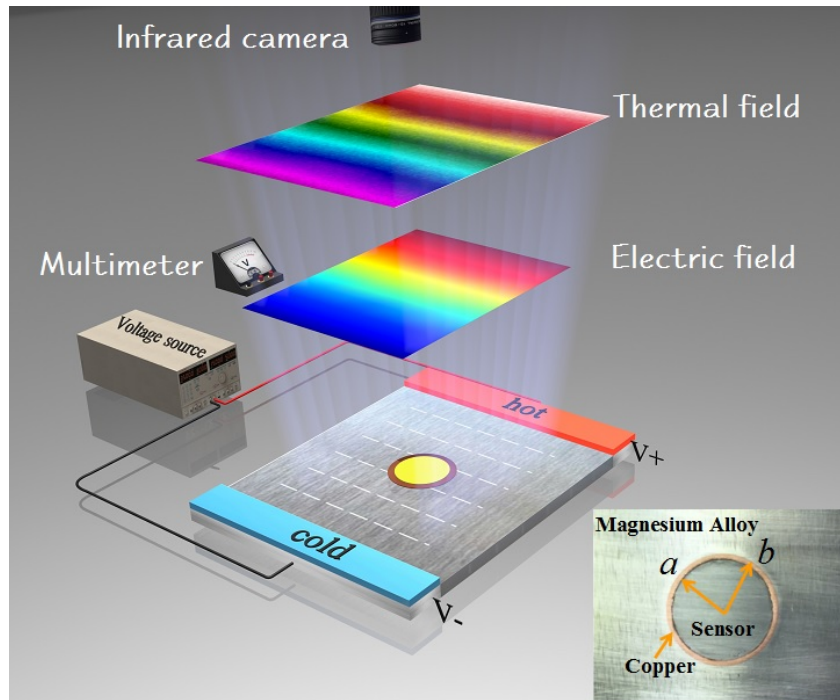


Figure 1. Schematic illustration of the 2D thermal and electric camouflage with unprocessed materials. In the experimental setup, the sensor, shell and the background are made of pure copper, stainless steel (ASTM 436) and magnesium alloy (AZ91D), respectively. The thermal and electric fields are applied on both ends of the sample. The inset shows the fabricated sample in greater detail. The geometrical parameters are $a=15\text{mm}$, $b=16.52\text{mm}$.

Figures 2

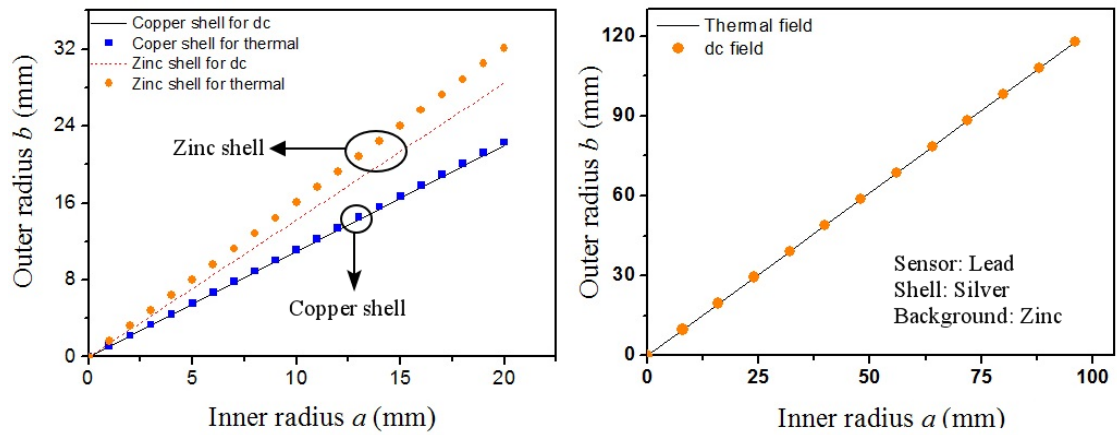


Figure 2. Calculated outer radius b as a function of inner radius a . The dual camouflaging capability can be achieved by tuning material and geometric parameters in electric and thermal fields. **(a)** Different shells for camouflage a sensor made of steel, inserted in a magnesium alloy plate. The solid black and blue dotted lines correspond to the calculated radius for the copper shell in dc and thermal fields, respectively. The orange markers and the red dotted line denote the calculated outer radius for zinc shell for thermal and dc fields, respectively. **(b)** Another example for designing the shell in dual-field using natural materials. A sensor made of lead, inserted in a zinc plate, can be camouflaged with a pure silver shell.

Figures 3

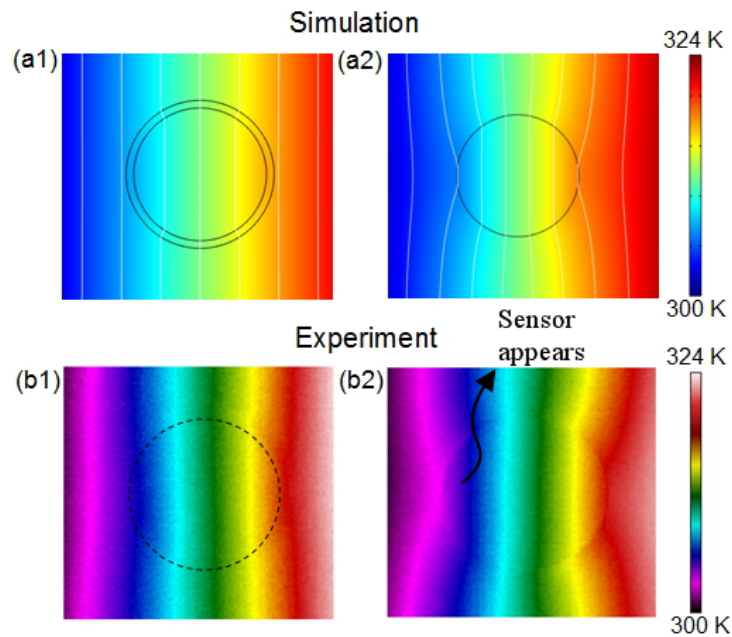


Figure 3 Calculated and measured *thermal field* distribution. **(a1)** Calculated thermal field distribution of a camouflaged sensor. **(a2)** Calculated thermal field distribution of a bare sensor. **(b1)** Measured thermal field distribution of a camouflaged sensor. The sensor, marked by black dotted cycle, is completely camouflaged in the surrounding environment. **(b2)** Measured thermal field distribution of the bare sensor. Without marking the position of sensor, a clear visible outline of the sensor is observed. The bare sensor can thus be easily detected by a thermal camera.

Figures 4

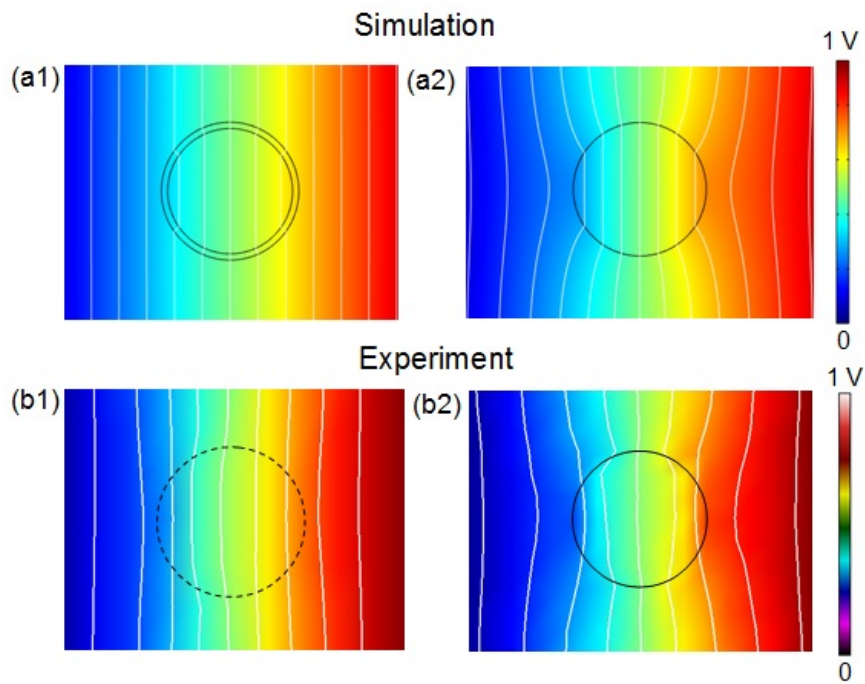


Figure 4 Calculated and measured *electric field* distribution. **(a1)** Calculated electric field distribution of the camouflaged sensor. **(a2)** Calculated electric field distribution of a bare sensor. **(b1)** Measured electric field distribution of the camouflaged sensor. The sensor, marked by black dotted cycle, is completely camouflaged in the surrounding environment. **(b2)** Measured electric field distribution of the bare sensor. A clear visible outline of the sensor is observed. It is therefore evident that the bare sensor may easily be detected by using electrical impedance scanning apparatus.

Figures 5

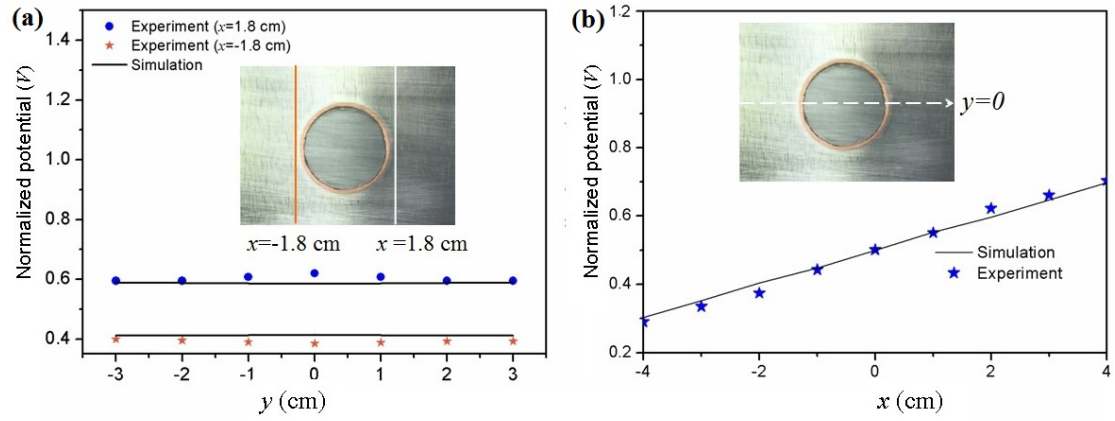


Figure 5. (a) Calculated and measured potential distribution of electric field along the lines $x = -1.8$ cm and $x = 1.8$ cm from the center of sensor. (b) Calculated and measured potential distribution of electric field along the line $x = 0$.

Supplementary materials - S1

Considering the electric and thermal conduction equations

$$\nabla \cdot (\kappa \nabla T) = 0, \quad \nabla \cdot (\sigma \nabla V) = 0 \quad (\text{S1})$$

Rewrite these two equations in a general form as

$$\nabla \cdot (\lambda \nabla \phi) = 0 \quad (\text{S2})$$

The general solutions ϕ_i in a cylindrical coordinate system can be expressed as

$$\phi_i = \sum_{n=1}^{\infty} [A_n^i r^n + B_n^i r^{-n}] \cos n\theta \quad (\text{S3})$$

where A_m^i and B_m^i are constants to be determined by boundary conditions. ϕ_i denotes the temperature and potential in different region: $i=1$ for the inner camouflaged region, $i=2$ for the shell and $i=3$ for the exterior region. As the temperature, electric fields and their normal components are continuous at the interface, we have

$$\phi_i \Big|_{r=a,b} = \phi_{i+1} \Big|_{r=a,b} \quad \lambda_i \frac{\partial \phi_i}{\partial r} \Big|_{r=b,c} = \lambda_{i+1} \frac{\partial \phi_{i+1}}{\partial r} \Big|_{r=b,c} \quad (\text{S4})$$

If we enforce the external signal enter the shell, we have $\lambda_3 = \lambda_b$, where λ_b is the conductivity of the background. Substituting Eq.(S3) into (S4) yields

$$b = a \sqrt{\frac{(\lambda_2 - \lambda_1)(\lambda_2 + \lambda_b)}{(\lambda_2 + \lambda_1)(\lambda_2 - \lambda_b)}} \quad (\text{S5})$$

Consider the conductivity λ_i to be electric and thermal conductivities ($\sigma_1, \sigma_2, \sigma_b, \kappa_1, \kappa_2, \kappa_b$), we can obtain Eq. (2) and (3) in main text.

The derived expression (S5) also can be obtained from neutral inclusion condition [32]

$$\lambda_b = \lambda_2 + \frac{2f_1\lambda_2(\lambda_1 - \lambda_2)}{2\lambda_2 + f_2(\lambda_1 - \lambda_2)} \quad (\text{S6})$$

where $f_1 = \frac{a^2}{b^2}$ and $f_2 = 1 - f_1$.

By solving b from (S6), one can also obtain (S5).

Supplementary materials - S2

A movie recorded for this dual camouflage device from 0 to 10 minutes can be found at URL:

<http://www.ece.nus.edu.sg/stfpage/eleqc/thermal-dc-camouflage.mov>